Temperature Dependence of Raman Scattering from Single-walled Carbon Nanotubes -Undefined Radial Breathing Mode Peaks at High Temperatures-

Shohei Chiashi[1], Yoichi Murakami[2], Yuhei Miyauchi[2] and Shigeo Maruyama[2]

[1] Department of Physics, School of Science, Tokyo University of Science, Shinjuku-ku, Tokyo 162-8601, Japan

[2] Department of Mechanical Engineering, School of Engineering, The University of Tokyo, Bunkyo-ku, Tokyo 113-8656, Japan

KEYWORDS: single-walled carbon nanotube, Raman scattering, temperature dependence, G-band peak, radial breathing mode peak, resonance Raman effect

ABSTRACT

We measured Raman scatterings from various single-walled carbon nanotube (SWNT) samples over a wide temperature range (4-1000 K). The G-band peaks showed clear temperature dependence, namely decrement in the Raman shift frequency and broadening of the peak width as temperature increases. The main G-band peak (G^+ peak) showed universal temperature dependence in Raman shift for the various SWNT samples and for the three excitation laser wavelengths (488.0, 514.5 and 632.8 nm), although the G-band features changed depending on SWNT samples and excitation laser wavelengths owing to resonance Raman effects. The Raman shift, peak width, and intensity of the RBM (radial breathing mode) peaks also exhibited temperature dependence. At high temperatures, undefined RBM peaks appeared, which could not be assigned to specific chiralities, and showed opposite temperature dependence in their intensities. Intensities of RBM peaks are strongly enhanced by resonance Raman effects, and the temperature may change the resonance Raman conditions.

1. Introduction

Raman scattering measurement is one of the useful analyses techniques in the characterization of SWNT samples and investigation of their properties.[1)] Raman scattering from SWNTs has unique features, the G-band, the D-band and radial breathing mode (RBM) peaks, which show the quality of SWNTs, the tube diameter distribution, etc. Raman scattering measurements are usually performed at room temperature (RT) and in atmospheric environment. Visible lasers are frequently used as Raman scattering excitation light, and because SWNTs absorb visible light the SWNT temperature is easily increased by laser irradiation. In particular, the SWNTs may be damaged or burned when high power excitation laser light is tightly focused with a high-magnification objective lens. When the SWNT temperature increases, the temperature dependence in Raman shift, peak width, and intensity would become significant, which makes it difficult to quantitatively analyze SWNT samples by Raman scattering.

Strong temperature dependences of Raman scattering spectra have been observed from in-situ measurements performed during the growth stage of SWNTs.[2)] Since the temperature of the sample changes from RT to the growth temperature (which is in 700 - 1000 °C) throughout the CVD process, understanding of the temperature dependence of Raman scattering over a wide range of temperature is essential in analyzing the in-situ Raman scattering spectra measured during the CVD process.

The temperature dependences have been measured in various carbon materials, such as SWNTs,[3-7)] multi-walled carbon nanotubes (MWNTs),[8)] double-walled carbon nanotubes (DWNTs)[6)] and graphite.[9)] In order to elucidate the temperature dependence of Raman scattering, it is important to control and measure the sample temperature. The sample temperature is typically controlled by sample stage heating (or cooling) or by laser irradiation heating. In the case of the sample stage temperature control, the sample's temperature could be equal to the stage's temperature, unless excitation laser light locally heats up the sample, or there exists a large temperature gap between the sample and the stage. In contrast, in the laser heating technique, it is difficult to directly measure the sample temperature within the laser spot. The sample temperature inside the laser spot could be measured by the temperature dependence of the intensity ratio between anti-stokes and stokes scattering if they were not strongly resonated.

Although some papers have reported the temperature dependence of Raman scattering for various SWNT samples, their results were slightly different from each other, as well as their temperature control and measurement techniques, excitation laser wavelengths, and temperature ranges. In the present paper, by using four kinds of SWNT samples (all samples were bundled SWNTs) and three excitation laser wavelengths (488.0, 514.5 and 632.8 nm), the temperature dependent measurements of SWNT Raman scattering were performed over a large temperature range (4 - 1000 K). All the experiments were performed in vacuum, in order to avoid damages to SWNTs and to reduce uncertainties regarding the temperature control and measurement.

2. Experimental

We used four types of SWNT samples. Two SWNT samples were produced by the ACCVD method; one was generated from Fe/Co metal catalyst particles supported with zeolite particles,[10)] and the other was generated from Co/Mo metal catalyst particles directly dispersed on a silicon (Si) wafer surface.[11)] Two additional SWNT samples were laser-oven SWNTs[12)]

synthesized from a carbon rod containing Ni/Co (0.6 at% each) at 1150 °C, and HiPco[13] SWNTs (batch #HPR113.4) supplied from Rice University.

Raman scatterings were measured at a controlled temperature while the SWNT samples were under vacuum. In the high temperature range (300 - 1000 K), the SWNTs were heated either by a Si heater or by the laser heating technique. The Si heater was a piece of Si wafer (Nilaco, (100), p-type, 15 × 5 × 0.5 mm), to which an AC voltage was applied to control its temperature by Joule-heating. The temperature of the Si heater was monitored with a thermocouple (chromel-alumel thermocouple, ϕ0.1 mm) and by the Raman shift of the Si peak (approximately at 520 cm^{-1} at RT), which downshifts continuously with increasing temperature.[14] The laser heating technique was used for SWNTs dispersed onto a small piece of Si (100 × 100 × 200 μm), where the heating laser was used also as the Raman excitation light. In this case, the temperature gap between inside and outside of the heating laser spot is thought to be negligible, because the size of the Si piece was sufficiently small and the thermal conductivity of Si is high (~120 W/m K at RT). The temperature of the piece was controlled by the laser power, and the temperature was monitored by the Raman peak of Si. For the low temperature range (4 - 300 K), samples were cooled by a helium refrigerator in vacuum.

Powdery SWNT samples (synthesized by ACCVD, laser-oven, and HiPco methods) were dispersed in ethanol and scattered onto the Si heater, the Si small piece for laser heating, or the sample stage of the helium refrigerator. Si pieces on which SWNTs were directly generated from Co/Mo particles by the ACCVD method were directly adhered onto the Si heater.

For Raman scattering measurements in the high temperature range, we used an environment controllable scanning probe microscope (SPM) unit (SII, SPA 300HV) built with a micro-Raman system (Seki Technotron).[2] The micro-Raman system was composed of an optical lens, a spectrometer (Chromex, 501is, 1200 or 1800 lines mm^{-1}) and a CCD (Andor, DV401-FI). An Ar^+ laser (488.0 and 514.5 nm) and a He-Ne laser (632.8 nm) were used as Raman excitation lasers, and Raman scattering was measured in backscattering configuration. In the low temperature range, a macro-Raman system, which was composed of an Ar^+ laser (488.0 nm) and a spectrometer (Nihon Bunko Kohgyo, CT-1000D, 1800 lines mm^{-1}) were used. In the temperature control with the Si heater and refrigerator, the power density of the excitation laser was about 10^4 mW/cm^2. This low laser intensity ensured minimal heating of SWNTs in the temperature control with the sample stages. The chamber of the SPM was evacuated (<10^{-7} Torr) by a turbo-molecular pump, preventing the SWNTs from oxidation at high temperature or condensation of water at low temperature.

3. Results

3.1. Temperature dependence of the G-band

Raman scattering spectra from SWNTs are composed of three major peaks, the G-band, the D-band and RBM peaks. Group theory predicts the G-band has six Raman-active modes,[15] where semi-conducting SWNTs exhibit four Lorentzian peaks corresponding to the E_2 (E_{2g}) and A (A_{1g}) + E_1 (E_{1g}) vibration modes, and metallic SWNTs exhibit two peaks (A (A_{1g}) modes), which have a Lorentzian lineshape and a Breit-Wigner-Fano (BWF) curve.[16-18] Figure 1(A) shows the temperature dependence in the Raman shift of the G^+ peaks ($A+E_1$ mode) (in the four kinds of SWNT samples) measured with three excitation lasers (488.0, 514.5 and 632.8 nm). Here, we decomposed the G-band spectra into five Lorentzian curves and a BWF curve. At high temperatures, the anharmonic components of bonding force become prominent owing to phonon-phonon

interactions. Then, the anharmonicity induces thermal expansion and decreases the force constant of bonds. In Raman scattering spectra, it broadens peak width, decreases intensity and decreases Raman shift frequency, which are known as the temperature dependence. The G-band peaks clearly showed the temperature dependence and the asymmetric properties of the BWF also appeared in the temperature dependence reported in Ref. 7. At RT, the G-band features are different for different samples, and the G^+ peak's Raman shifts were slightly different around 1592 cm^{-1} depending on SWNT samples. However, all G^+ peaks show similar temperature dependence in Raman shift, as shown in Fig. 1(A), regardless of the type of the sample. The Raman shift of the G^+ peak shows universal temperature dependence, independent of SWNT sample type or excitation laser wavelength, thus the temperature of any SWNT sample could be measured from the change in the Raman shift of the G^+ peak.

The dash line in Fig. 1(A) was a fitting line represented by the following equation, [19)]

$$\omega(T) = \omega_0 - \frac{A}{\exp(B\hbar\omega_0/k_B T) - 1} \qquad (1).$$

Here, $\hbar$ is the Planck's constant, k_B is the Boltzmann constant and T is the sample temperature. With ω_0 = 1594 cm^{-1}, A = 38.4 cm^{-1} and B = 0.438, the fitting line agreed with the present data in Fig. 1(A). Cui *et al.*[19)] expressed the temperature dependence of the diamond Raman peak by using the equation (1), based on the discussion of Balkanski *et al.*. [14)] Later, the same formula was also employed for the analysis of the temperature dependence of the E_2 phonon frequency of GaN.[20)] The best-fit value B was quite close to 0.5 for our G^+ band, which suggested that the temperature dependence of the G^+ peak was mainly derived from three-phonon scattering process.[14)] However, since the equation (1) was regarded as purely empirical formula, which could contain the contribution of electron-phonon interaction,[19)] more detail speculation is difficult at this stage.

The laser heating technique was another temperature control method used for SWNTs. HiPco samples were dispersed onto a small Si piece, and the G-band was measured with various laser powers (~60 mW). From RT to 1000 K, the temperature of SWNTs, which was calculated from the position of the G^+ peak, agreed with the temperature of the Si piece, which was also calculated from the Si's Raman peak. Because the thermal resistance between the SWNTs and the Si piece is reasonably assumed to be smaller than that between SWNTs and the environment, and the thermal conductivity of Si is high even at high temperature, there was no temperature difference between the Si piece and SWNTs. Moreover, the samples could reach high temperatures (~1000 K) with relatively low laser power (~60 mW), because the small surface area of the Si piece results in small thermal radiation from its surfaces as well as small heat transfer from its bottom surface to the support. In this case, the laser heating technique was also convenient for the temperature control of SWNTs.

Figure 1(B) shows the difference in Raman shift between the G^+ and G^- peaks (A (A_{1g}) + E_1 (E_{1g}) mode), which are dominant peaks in the G-band at various temperatures. At RT, the Raman shift of the G^- peak changed with excitation laser wavelength, because SWNTs with different diameter are in resonance and the Raman shift of the G^- peak is dependent on the tube's diameter. Therefore, the difference between the G^+ and G^- peaks' Raman shift is related to the diameter of semi-conducting SWNTs, and is described by[21)]

$$G^+ - G^- = \alpha / d_{tube}^{\,2} \qquad (2)$$

where d_{tube} is the SWNT diameter (nm) and α is the proportionality coefficient. Although the differences were almost constant for 632.8 nm excitation laser, slight increases were observed in the case of the 488.0 and 514.5 nm excitation lasers, which suggested that at high temperatures, relatively smaller-diameter semi-conducting SWNTs were resonantly excited with 488.0 and 514.5 nm, owing to the resonance condition changing with the temperature.

3.2. Temperature dependence of RBM peaks

RBM peaks are also dependent on the temperature.[3-5] Figure 2 shows Raman scattering from HiPco samples at various temperatures measured with 488.0, 514.5 and 632.8 nm excitation lasers. Since many peaks overlap in the low frequency range (150 - 350 cm^{-1}), the spectra were decomposed into Lorentzian curves. Thus far, several experimental and theoretical studies on the optical properties of isolated SWNTs have assigned chiral indices (n, m) corresponding to respective RBM peaks. We adopted the sets of chiral assignment reported in Refs. 22 and 23, and applied it to our result assuming that the positions of RBM peaks of isolated SWNTs are not different from those of bundled SWNTs.[23] We also adopted the relationship between the diameter and the Raman shift described by[24]

$$\omega_{RBM} = 248/d_{tube} \qquad (3)$$

where ω_{RBM} is the Raman shift (cm^{-1}). Most of the observed peaks are assigned with their chiral indices as shown in Fig. 2. However, some peaks, whose intensities were very weak (or nearly unobservable) at RT, could not be assigned when the resonance window width was 0.1 eV.[25] Such unassigned peaks, which we called “undefined” peaks, were labeled with “peak X” (X=A, B, C…) instead a of chiral index (n, m) in Fig. 2(A, B). On the contrary, the spectra in Fig. 2(C) could not be decomposed into Lorentzian curves corresponding to the chirality assignments, because peaks appeared around 200 cm^{-1} could not be resolved well with the spectral resolution of our monochromator. For all peaks, including the undefined peaks, the Raman frequency downshifted and the peak width increased with increasing temperature, where the downshifting rates ranged from -0.001 to -0.015 cm^{-1}/K.

Strictly, it is impossible to compare absolute Raman intensities of two different spectra. However, we think the intensities of the Raman spectra shown in Fig. 2 can be reasonably compared because the measurement conditions (e.g., the laser spot position on the sample, the distance between the objective lens and the sample, the laser power, and the exposure time) were kept the same throughout the measurements. Figure 3(A) shows temperature dependence of the normalized integral intensities, which are the product of intensity and peak width normalized by those at RT. The integral intensities of the peaks that were assigned to chiral indices (“normal” RBM peaks), decreased with increasing temperature, while those of the undefined peaks apparently increased.

The intensity ratio between the stokes and anti-stokes Raman scattering was expressed by

$$\frac{I_{AS}}{I_S} = \frac{R_{AS}}{R_S}\left(\frac{\omega_{AS}}{\omega_S}\right)^3 \exp\left(-\frac{\hbar\omega_{RBM}}{k_B T}\right) \qquad (4)$$

where I_{AS} and I_S are anti-stokes and stokes Raman scattering intensities, respectively,
and R_{AS} and R_S are corresponding resonance Raman factors and ω_{AS} and ω_S are Raman scattering wavenumbers. Raman scattering from SWNTs is strongly affected by resonance Raman effects, and hence the resonance Raman factors (R_{AS} and R_S) are important. Here, these factors were calculated

using the following equation[23, 25)]

$$R(E_l) \propto \left| \frac{1}{(E_l - E_{ii} - i\Gamma)(E_l \pm E_{ph} - E_{ii} - i\Gamma)} \right|^2 \quad (5)$$

where E_l is energy of the excitation laser, Γ is the width of the resonance window, E_{ph} is the phonon energy, E_{ii} is the electronic transition energy, and the + (-)symbol applies to the anti-stokes (stokes) process. Figure 3(B) shows the temperature dependence in the resonance factor ratio (R_{AS}/R_S) between stokes and anti-stokes scattering measured with a 488.0 nm excitation laser. The resonance factor ratio represents the magnitude relation between the transition energy (E_{ii}) and the excitation laser energy (E_l) according to equation (5), although absolute values of the transition energies are unknown. It is more (less) than 1.0 when the transition energy is smaller (larger) than the excitation laser energy. With increasing temperature, the ratio of all peaks would tend to converge to 1.0 as shown in Fig. 3(B). While the transition energies of semi-conducting SWNTs were reported to change with temperature according to their chiralities,[23)] this convergence of the resonance factor ratio could be explained by the broadening of the resonance window width, instead of a shift the transition energies, in equation (5).

The undefined peaks show the same temperature dependence in Raman shift and peak width as normal RBM peaks, as well as the resonance factor ratio as shown in Fig. 3(B). Moreover, one of the undefined peaks, which was corresponding to “peak B” in Fig. 2(A), was observed from SWNTs that consisted of carbon-13. [26)] The SW^{13}CNTs were synthesized with ACCVD method by using ^{13}C ethanol as carbon source and Fe/Co catalysts on zeolites. Their Raman spectra, including “peak B”, clearly showed the isotope shift, therefore, we assume that the undefined peaks are also RBM peaks, although their intensities show extraordinary temperature dependence.

Figure 4 shows a Kataura plot for obtained data, which were reported in Refs. 22 and 23. Here, we added plots whose transition energies were estimated from the resonance Raman factor ratio of the normal RBM peaks measured with 488.0 (blue open circles) and 514.5 nm (green open diamonds) excitation lasers at RT. These data points show good agreement with points on the Kataura plot. Similarly, we plotted the undefined RBM peaks. The points of these peaks did not correspond to any of those on the Kataura plot, although they were within the width of the resonance window (Γ) from the excitation laser energies. One of the possible reasons why the undefined RBM peaks appeared and their intensities increased with increasing temperature is resonance transitions caused by absorption of light polarized perpendicular to the tube axis (E_{ij} ($i \neq j$) transition).[27)] Although this transition is suppressed at RT by the depolarization effect,[28)] the temperature increase might moderate the depolarization effects in bundled SWNTs.

4. Summary

Raman scatterings from various bundled SWNT samples have been measured using three excitation laser wavelengths (488.0, 514.5 and 632.8 nm) over a wide temperature range (4 - 1000 K). The Raman shift of the G^+ peak exhibited universal temperature dependence for all SWNT samples and all excitation wavelengths investigated, and hence the temperature of SWNT samples can conveniently be measured based on the changes in the G^+ peak position. The RBM peaks also showed temperature dependences, such as downshifts of the Raman frequency, broadening of the peak width, and reduction in the intensities with increasing temperature. Furthermore, we have shown the existence of several RBM peaks that could not be assigned to any chiral indices, and have

found that the intensities of those unassigned peaks were very weak at RT and increased with increasing temperature.

ACKNOWLEDGMENTS

The authors thank Mr. M. Sunose (Seki Technotron Corp.) for assistance in designing the Raman scattering measurement system and Prof. R. E. Smalley (Rice University) for supplying HiPco samples. Part of this work was financially supported by KAKENHI #19206024 and #19054003 from JSPS and SCOPE #051403009 from MIC

REFERENCES

1 R. Saito, G. Dresselhaus, M. S. Dresselhaus: *Physical Properties of Carbon Nanotubes* (Imperial College Press, London, 1998).

2 S. Chiashi, Y. Murakami, Y. Miyauchi, S. Maruyama: Chem. Phys. Lett. **386** (2004) 89.

3 H. D. Li, K. T. Yue, Z. L. Lian, Y. Zhan, L. X. Zhou, S. L. Zhang, Z. J. Shi, Z. N. Gu, B. B. Liu, R. S. Yang, H. B. Yang, G. T. Zou, Y. Zhang, S. Iijima: Appl. Phys. Lett. **76** (2000) 2053.

4 N. R. Raravikar, P. Keblinski, A. M. Rao, M. S. Dresselhaus, L. S. Schadler, P. M. Ajayan: Phys. Rev. B **66** (2002) 235424.

5 M. N. Iliev, A. P. Litvinchuk, S. Arepalli, P. Nikolaev, C. D. Scott: Chem. Phys. Lett. **316** (2000) 217.

6 Z. P. Zhou, L. Ci, L. Song, X. Q. Yan, D. F. Liu, H. J. Yuan, Y. Gao, J. X. Wang, L. F. Liu, W. Y. Zhou, S. S. Xie, Y. X. Du, Y. J. Mo: Chem. Phys. Lett. **396** (2004) 372.

7 T. Uchida, M. Tachibana, S. Kurita, K. Kojima: Chem. Phys. Lett. **400** (2004) 341.

8 F. M. Huang, K. T. Yue, P. H. Tan, S. L. Zhang, Z. J. Shi, X. H. Zhou, Z. N. Gu: J. Appl. Phys. **84** (1998) 4022.

9 P. H. Tan, Y. M. Deng, Q. Zhao, W. C. Cheng: Appl. Phys. Lett. **74** (1999) 1818.

10 S. Maruyama, R. Kojima, Y. Miyauchi, S. Chiashi, M. Kohno: Chem. Phys. Lett. **360** (2002) 229.

11 Y. Murakami, Y. Miyauchi, S. Chiashi, S. Maruyama: Chem. Phys. Lett. **377** (2003) 49.

12 A. Thess, R. Lee, P. Nikolaev, H. J. Dai, P. Petit, J. Robert, C. H. Xu, Y. H. Lee, S. G. Kim, A. G. Rinzler, D. T. Colbert, G. E. Scuseria, D. Tomanek, J. E. Fischer, R. E. Smalley: Science **273** (1996) 483.

13 P. Nikolaev, M. J. Bronikowski, R. K. Bradley, F. Rohmund, D. T. Colbert, K. A. Smith, R. E. Smalley: Chem. Phys. Lett. **313** (1999) 91.

14 M. Balkanski, R. F. Wallis, E. Haro: Phys. Rev. B **28** (1983) 1928.

15 M. A. Pimenta, A. Marucci, S. D. M. Brown, M. J. Matthews, A. M. Rao, P. C. Eklund, R. E. Smalley, G. Dresselhaus, M. S. Dresselhaus: J. Mater. Res. **13** (1998) 2396.

16 A. M. Rao, E. Richter, S. Bandow, B. Chase, P. C. Eklund, K. A. Williams, S. Fang, K. R. Subbaswamy, M. Menon, A. Thess, R. E. Smalley, G. Dresselhaus, M. S. Dresselhaus: Science **275** (1997) 187.

17 H. Kataura, Y. Kumazawa, Y. Maniwa, I. Umezu, S. Suzuki, Y. Ohtsuka, Y. Achiba: Synth. Met. **103** (1999) 2555.

18 S. D. M. Brown, A. Jorio, P. Corio, M. S. Dresselhaus, G. Dresselhaus, R. Saito, K. Kneipp: Phys. Rev. B **6315** (2001) 155414.

19 J. B. Cui, K. Amtmann, J. Ristein, L. Ley: J. Appl. Phys. **83** (1998) 7929.

20 Y. Ohno, M. Akita, S. Kishimoto, K. Maezawa, T. Mizutani: Jpn. J. Appl. Phys. **41** (2002) L452.

21 A. Jorio, A. G. Souza, G. Dresselhaus, M. S. Dresselhaus, A. K. Swan, M. S. Unlu, B. B. Goldberg, M. A. Pimenta, J. H. Hafner, C. M. Lieber, R. Saito: Phys. Rev. B **65** (2002) 155412.

22 H. Telg, J. Maultzsch, S. Reich, F. Hennrich, C. Thomsen: Phys. Rev. Lett. **93** (2004) 177401.

23 C. Fantini, A. Jorio, M. Souza, M. S. Strano, M. S. Dresselhaus, M. A. Pimenta: Phys. Rev. Lett. **93** (2004) 147406.

24 A. Jorio, R. Saito, J. H. Hafner, C. M. Lieber, M. Hunter, T. McClure, G. Dresselhaus, M. S. Dresselhaus: Phys. Rev. Lett. **86** (2001) 1118.
25 A. Jorio, A. G. Souza, G. Dresselhaus, M. S. Dresselhaus, R. Saito, J. H. Hafner, C. M. Lieber, F. M. Matinaga, M. S. S. Dantas, M. A. Pimenta: Phys. Rev. B **6324** (2001) 245416.
26 Y. Miyauchi, S. Maruyama: Phys. Rev. B **74** (2006) 035415.
27 A. Gruneis, R. Saito, J. Jiang, G. G. Samsonidze, M. A. Pimenta, A. Jorio, A. G. Souza, G. Dresselhaus, M. S. Dresselhaus: Chem. Phys. Lett. **387** (2004) 301.
28 H. Ajiki, T. Ando: Physica B **201** (2004) 349.

FIG. 1 (A) Temperature dependence of Raman shifts of the G^+ peaks for various SWNT samples measured with a 488.0 nm excitation laser and for HiPco sample measured with three excitation lasers (488.0, 514.5 and 632.8 nm). The dash line is a fitting line calculated using the equation (1). (B) Temperature dependence of the differences between G^+ and G^- peaks, measured with the three excitation lasers.

FIG. 2 RBM peaks (150 - 350 cm^{-1}) for HiPco samples at various temperatures. Excitation laser wavelengths were (A) 488.0, (B) 514.5 and (C) 632.8 nm, respectively.

FIG. 3(A) Integral normalized intensities of RBM peaks measured with a 488.0 nm excitation laser. The integral normalized intensities were a product of intensities and peak width, normalized by those at RT. (B) Resonance Raman factor ratio between anti-stokes and stokes Raman scattering intensities at various temperatures. The ratio for all RBM peaks tended to converge.

FIG. 4 Relationships between Raman shift and the estimated transition energies of RBM peaks, measured with 488.0 and 514.5 nm excitation lasers (blue circles and green diamonds). The open and filled marks denote the normal and the undefined RBM peaks, respectively. For reference, the open triangles and open squares show points reported in Refs. 22 and 23.

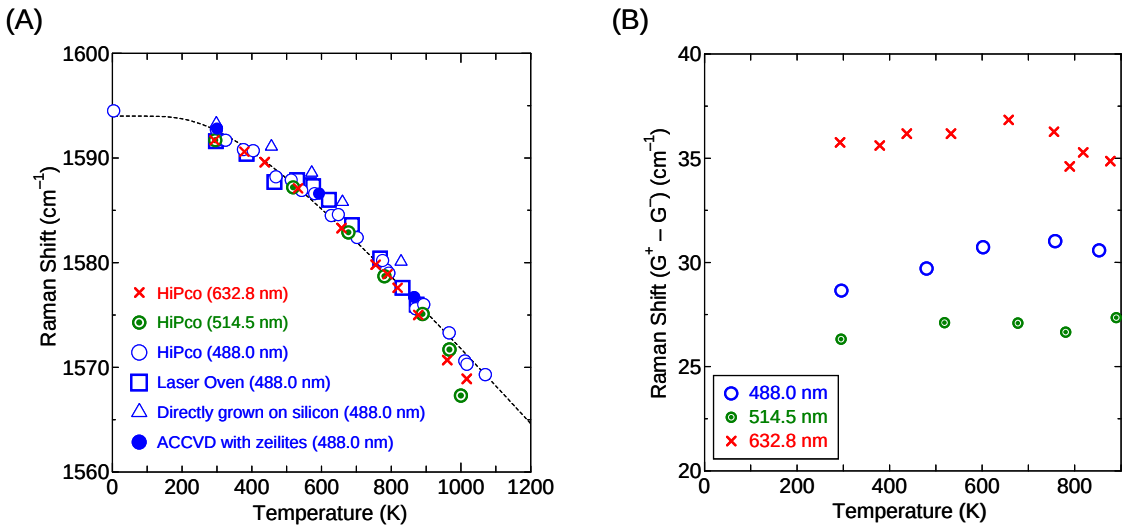
(A)
(B)
Raman Shift (cm^{-1})
Temperature (K)
HiPco (632.8 nm)
HiPco (514.5 nm)
HiPco (488.0 nm)
Laser Oven (488.0 nm)
Directly grown on silicon (488.0 nm)
ACCVD with zeilites (488.0 nm)
Raman Shift (G$^+$ – G$^-$) (cm^{-1})
488.0 nm
514.5 nm
632.8 nm

FIG. 1

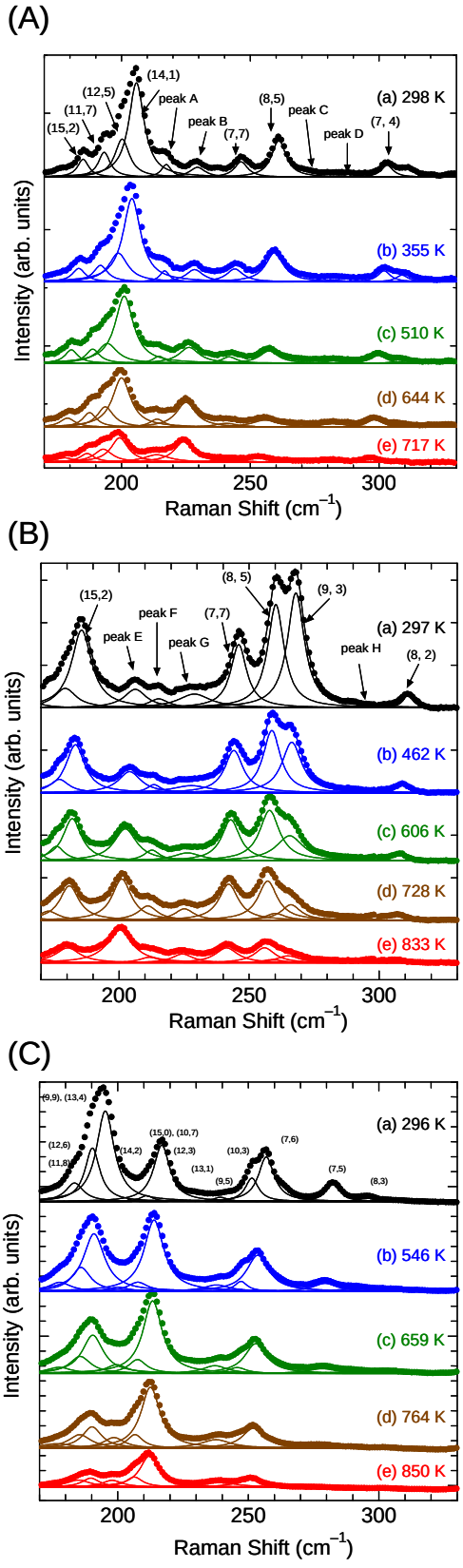
(A)
(14,1)
(12,5)
(11,7)
(15,2)
peak A
peak B
(7,7)
(8,5)
peak C
peak D
(7, 4)
(a) 298 K
(b) 355 K
(c) 510 K
(d) 644 K
(e) 717 K
Intensity (arb. units)
200
250
300
Raman Shift (cm^{-1})
(B)
(15,2)
peak E
peak F
peak G
(7,7)
(8, 5)
(9, 3)
peak H
(8, 2)
(a) 297 K
(b) 462 K
(c) 606 K
(d) 728 K
(e) 833 K
Intensity (arb. units)
200
250
300
Raman Shift (cm^{-1})
(C)
(9,9), (13,4)
(12,6)
(11,8)
(14,2)
(15,0), (10,7)
(12,3)
(13,1)
(9,5)
(10,3)
(7,6)
(7,5)
(8,3)
(a) 296 K
(b) 546 K
(c) 659 K
(d) 764 K
(e) 850 K
Intensity (arb. units)
200
250
300
Raman Shift (cm^{-1})

FIG. 2

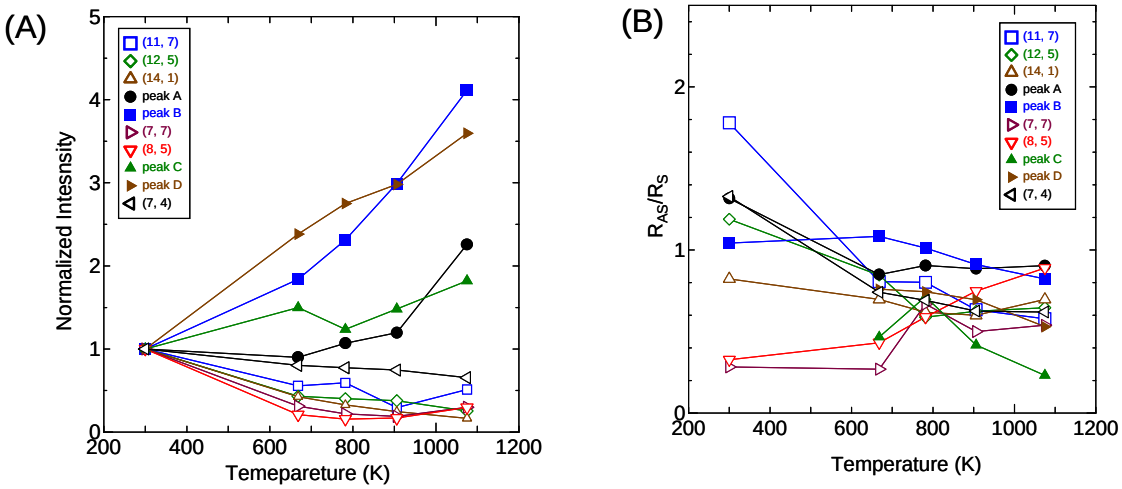
(A)
Normalized Intesnsity
Temepareture (K)
(11, 7)
(12, 5)
(14, 1)
peak A
peak B
(7, 7)
(8, 5)
peak C
peak D
(7, 4)
(B)
R_{AS}/R_S
Temperature (K)

FIG. 3

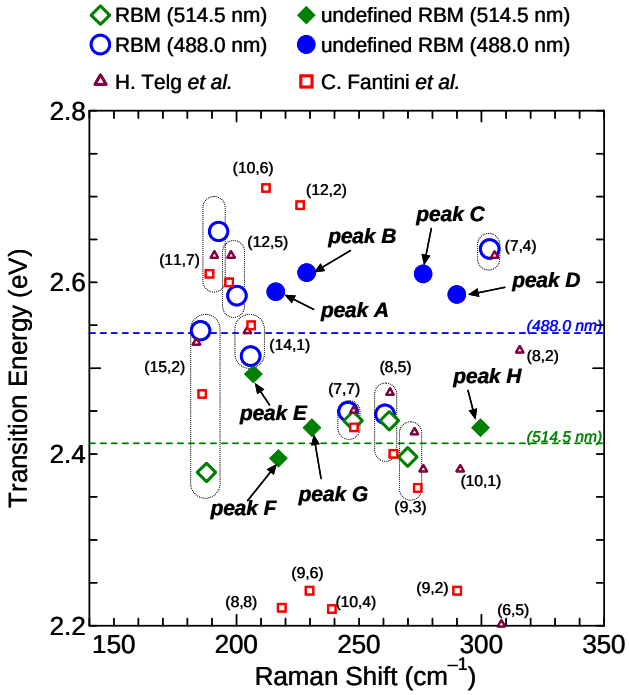
RBM (514.5 nm)
undefined RBM (514.5 nm)
RBM (488.0 nm)
undefined RBM (488.0 nm)
H. Telg et al.
C. Fantini et al.
Transition Energy (eV)
Raman Shift (cm^{-1})
peak A
peak B
peak C
peak D
peak E
peak F
peak G
peak H
(488.0 nm)
(514.5 nm)
(10,6)
(12,2)
(11,7)
(12,5)
(7,4)
(14,1)
(8,2)
(15,2)
(8,5)
(7,7)
(10,1)
(9,3)
(9,6)
(8,8)
(10,4)
(9,2)
(6,5)

FIG. 4